Fluctuations in turbulent Rayleigh–Bénard convection: The role of plumes

Siegfried Grossmann[a)]
Department of Physics, University of Marburg, Renthof 6, D-35032 Marburg, Germany

Detlef Lohse[b)]
Department of Applied Physics, University of Twente, 7500 AE Enschede, The Netherlands

Our unifying theory of turbulent thermal convection [Grossmann and Lohse, J. Fluid. Mech. **407**, 27 (2000); Phys. Rev. Lett. **86**, 3316 (2001); Phys. Rev. E **66**, 016305 (2002)] is revisited, considering the role of thermal plumes for the thermal dissipation rate and addressing the local distribution of the thermal dissipation rate, which had numerically been calculated by Verzicco and Camussi [J. Fluid Mech. **477**, 19 (2003); Eur. Phys. J. B **35**, 133 (2003)]. Predictions for the *local* heat flux and for the temperature and velocity fluctuations as functions of the Rayleigh and Prandtl numbers are offered. We conclude with a list of suggestions for measurements that seem suitable to verify or falsify our present understanding of heat transport and fluctuations in turbulent thermal convection. © *2004 American Institute of Physics.* [DOI: 10.1063/1.1807751]

I. INTRODUCTION

Turbulent Rayleigh–Bénard convection is one of the classical problems of fluid dynamics. For recent reviews we refer to Refs. 1 and 2; for an earlier review to Ref. 3.

One of the key questions is: How do the Nusselt (Nu) and the wind Reynolds (Re) number depend on the Rayleigh (Ra) and Prandtl (Pr) number? (The dependence on the aspect ratio Γ is not considered here; we take $\Gamma = 1$. Predictions on the aspect ratio dependence of Nu and Re have been given in Ref. 4.) For a long time it had been believed that there were power law dependences of Nu and Re on Ra and Pr, though there was a fierce debate on the values of the power law exponents. Recent experiments by various groups[5–12] seem to suggest that the Ra and Pr dependences in general are more complicated than simple power laws. This finding has been predicted by our recent unifying theory on turbulent thermal convection.[13–15]

In that theory the volume averaged kinetic dissipation rate $\epsilon_u = \nu \langle [\partial_i u_j(\boldsymbol{x}, t)]^2 \rangle_{V,t}$ and the thermal dissipation rate $\epsilon_\theta = \kappa \langle [\partial_i \theta(\boldsymbol{x}, t)]^2 \rangle_{V,t}$ are split into their boundary and bulk parts, which are then modeled with the corresponding length, velocity, and temperature scales in the bulk or boundary layer, respectively. This leads to certain scaling behaviors of the individual terms of the balances $\epsilon_u = \epsilon_{u,bulk} + \epsilon_{u,\mathrm{BL}}$ and $\epsilon_\theta = \epsilon_{\theta,bulk} + \epsilon_{\theta,\mathrm{BL}}$, but not to pure scaling of Nu(Ra,Pr) (see Fig. 2 of Ref. 14) and Re(Ra,Pr) (see Fig. 3 of Ref. 15).

Though we are not aware of experiments which are inconsistent with our theoretical results for Nu(Ra,Pr) and Re(Ra,Pr), there is a recent numerical finding that requires reconsideration of our theory: Verzicco and Camussi[16] and Verzicco[17] numerically found that the ratio of $\epsilon_{\theta,\mathrm{BL}}$ and $\epsilon_{\theta,bulk}$ is basically independent of Ra, whereas our theory suggests that the bulk part of the thermal dissipation rate should take over for large Ra. The theory also says that the latter is true

in the case of the *kinetic* dissipation rate ϵ_u. Here the numerical simulations[16] indeed show that for the kinetic dissipation rate the bulk contribution becomes dominant for large Ra, just as our theory predicts.

In Sec. II we will make a suggestion how one might properly include also the *thermal plumes*, in addition to the thermal boundary layers on the top and bottom plates. We understand these plumes as *detached* thermal boundary layer. Correspondingly, both thermal plumes and thermal boundary layer are assumed to have the same characteristic length scale, namely λ_θ, the thickness of the thermal boundary layer. Following this thought, the thermal dissipation rate ϵ_θ can then be split into two differently scaling contributions: the thermal dissipation due to the plumes *pl* together with the smooth parts of the BL $\epsilon_{\theta,pl}$ and the thermal dissipation $\epsilon_{\theta,bg}$ of the turbulent background *bg*,

$$\epsilon_\theta = \epsilon_{\theta,bg} + \epsilon_{\theta,pl}. \tag{1}$$

Thermal plumes seem to be extended in the direction in which they are advected.[18] The observations reported in Refs. 18 and 19 suggest that the thermal plumes are mainly sheet-like structures rather than mushroom-like structures, which would occur from a point-wise heat source. The same is suggested by numerical simulations of thermal convection by F. Toschi (private communication). Funfschilling and Ahlers[18] explain the sheet-like structures with the flow organization in the thermal BL just beyond the onset of convection therein. This flow organization is in rolls.[20] It is the extension in the second dimension which makes their experimental detection easier and more likely. The plume signatures will be discussed in Sec. II C.

Equation (1) turns out to be a slight modification or extension of our previous interpretation only, namely, the inclusion of the "detached" boundary layers (plumes) in the thermal dissipation rate. There will be no change in our previous quantitative results for Nu and Re as functions of Ra and Pr.

The physical reason behind this splitting into *bg* and *pl* contributions is the close relation of ϵ_θ with the heat flux Nu.

[a)]Electronic mail: grossmann@physik.uni-marburg.de
[b)]Electronic mail: d.lohse@utwente.nl

Based on our unifying theory, we are able to make predictions on the heat flux carried by the turbulent background fluctuation and by the plumes (Sec. III). If one wants to check these predictions against experiments, one of course must develop an algorithm to separate the plume events in time series of the temperature (and possibly of the simultaneous transversal velocity) from the turbulent background. Recently, Ching et al. developed such algorithm.[21] Similar algorithms have been developed by Sreenivasan and co-workers.[22] Based on the splitting of the flow in plume and background contributions, we can make predictions for the local heat flux at the sidewalls (which is plume dominated) and the local heat flux in the center (which is turbulent background dominated).

The second issue we want to address in this paper are the temperature and the velocity fluctuations (Sec. IV), extending our considerations of Sec. V of Ref. 4. In our unifying theory[13–15] we have expressed the kinetic and the thermal dissipation rates in terms of large scale quantities characterizing the energy input rates. However, the dissipation rates are also connected with the small scale local fluctuations, relevant for the energy dissipation or "output" rate. We will use the results from our unifying theory to make predictions how the fluctuations should depend on both Ra and Pr. It will turn out to be useful and necessary to distinguish between the thermal background fluctuations θ'_{bg} and the thermal fluctuations caused by plumes θ'_{pl}, similarly as done by Wunsch and Kersten.[23] The total thermal fluctuations θ' are described by the root mean square of the sum of both,

$$(\theta')^2 = (\theta'_{bg})^2 + (\theta'_{pl})^2. \tag{2}$$

Depending on where in the cell the fluctuations are measured, they will be either dominated by the plume fluctuations or by the background fluctuations. The photographs and movies of the Xia and Tong groups (see, e.g., Ref. 24, in particular, Fig. 2 of that paper) suggest that the sidewalls are plume dominated, and the center is background dominated, potentially leading to different scaling behaviors. Indeed, that fluctuations can scale differently at different locations in the cell has been found by Daya and Ecke.[25,26] Most Ra and Pr number dependences for the temperature and velocity fluctuations found in those papers will turn out to be consistent with our predictions. However, the Pr dependence of θ' found in Ref. 26 is definitely stronger than what we will obtain within our theory. We cannot resolve this discrepancy. So we present our theoretical prediction and suggest to remeasure $\theta'(\mathrm{Pr})$ in a larger Pr range and at different locations in the cell.

Section V contains a summary of the paper and an extended list of suggestions for measurements, which seem suitable to verify or falsify our theoretical framework for the understanding of the heat fluxes and the fluctuations in turbulent thermal convection.

The main feature of our reconsideration of the global transport properties and of the local fluctuations is that the role of thermal plumes has been stressed more than we did before. Thermal plumes have long been known to occur in thermal convection. Their life-cycle had been visualized by Zocchi et al.[27] and they played a prominent role in the Chi-

cago thermal convection theory.[28] We had viewed it as a strong point of our theory that no statement on the plumes was necessary, but perhaps after all one has to realize that plumes play a really important role for both the heat transfer and the fluctuations.

II. REVISITING OUR UNIFYING THEORY OF THERMAL CONVECTION

A. Decomposition of dissipation rates

As stated already in the Introduction, the main idea is to split the kinetic dissipation rate into its boundary and bulk contributions, whereas the thermal dissipation rate is partitioned into the turbulent background and plume contributions,

$$\epsilon_u = \frac{\nu^3}{L^4}(\mathrm{Nu}-1)\mathrm{RaPr}^{-2} = \epsilon_{u,\mathrm{BL}} + \epsilon_{u,bulk}, \tag{3}$$

$$\epsilon_\theta = \kappa \frac{\Delta^2}{L^2}\mathrm{Nu} = \epsilon_{\theta,pl} + \epsilon_{\theta,bg}. \tag{4}$$

The first equality in each row represents an exact relation which can be obtained from the Boussinesq equations by integrating the respective dissipation rate over the whole volume of the cell, employing the respective boundary conditions (cf., e.g., Ref. 3). The relations of course only hold in the limit of ideal boundary conditions.

B. Kinetic dissipation rate

The kinetic dissipation rates are modeled just as in Refs. 13–15, namely, as

$$\epsilon_{u,\mathrm{BL}} \sim \nu \frac{U^2}{\lambda_u^2} \frac{\lambda_u}{L} \tag{5}$$

and

$$\epsilon_{u,bulk} \sim U^3/L, \tag{6}$$

respectively. Here U is the large scale wind velocity (defining $\mathrm{Re}=UL/\nu$), and λ_u is the kinetic BL width both at the plates and at the sidewalls. We consider the BL as of Blasius–Prandtl type, as long as there is no transition to turbulence in the BL. Then $\lambda_u \sim L/\sqrt{\mathrm{Re}}$, cf. Refs. 29 and 30 and Sec. II D 1. For the kinetic bulk dissipation it is argued that it should equal the large scale input, which is caused by the large scale wind. That wind of course has its origin in the heating, but by self-consistently solving Eqs. (3) and (4) this is automatically considered, just as explained in Refs. 13 and 14 in detail. Recently it has been shown[31] that in fact it is the thermal plumes which initiate the wind.

C. Plumes as detached thermal BL

We now model the two contributions to the thermal dissipation rates in the decomposition (4). Consider first the thermal dissipation rate due to the smooth parts of the thermal BL and the plumes (detached thermal BL). For small degree of convective turbulence this is the more relevant contribution. Our ansatz is

$$\epsilon_{\theta,pl} \sim \kappa \frac{\Delta^2}{\lambda_\theta^2} \frac{\lambda_\theta}{L} N_{pl}^{sheet}. \tag{7}$$

Here we have assumed that the smooth parts of the thermal BL and the plumes have the typical temperature Δ and that the typical scale of changes is the thermal boundary layer width λ_θ.

The factor λ_θ/L in Eq. (7) is a geometric factor, representing the volume ratio of the thermal BL or the detached thermal BL (plumes) to the total volume. It reflects the idea that the characteristic width of a plume scales in the same way as the thermal boundary layer does. For the thermal BL this seems obvious. For the detached thermal BL (plumes) it implies that a lateral extension of length $\sim L$ has been assumed, i.e., that the *relevant* structures for the thermal dissipation are mainly *sheet-like* rather than mushroom-like, at least initially, when they detach from the thermal BL. Later, they may decay to mushroom-like structures, whose number then is of order L/λ_θ. Indeed, sheet-like structures have been observed in various experiments and simulations.[18,19,27] *Originially* mushroom-like structure (as also seen in experiments and simulations[19,27,31,32]) may occur, too, but for them the corresponding geometric factor would be $(\lambda_\theta/L)^2$, i.e., of higher order (in λ_θ/L) correction as compared to the two-dimensional sheet-like structures. Therefore, they are less relevant for the thermal dissipation caused by the plumes. In Sec. III A we will give a further argument that the sheet-like structures are the relevant ones for the thermal dissipation (7) and in Sec. II G we offer a physical mechanism for the evolvement of the sheets out of the thermal BLs.

Finally, the last factor N_{pl}^{sheet} in Eq. (7) represents the average number of sheet-like plumes being around. Note that upper and lower thermal BL are included in this number as two pronounced sheets. N_{pl}^{sheet} is expressed and calculated from the plume shedding frequency f_{shed} and the average plume lifetime τ_{pl},

$$N_{pl}^{sheet} \sim f_{shed} \tau_{pl}. \tag{8}$$

The plume lifetime τ_{pl}, in which it looses its temperature contrast by thermal diffusivity, is determined by the thickness λ_θ of the (detached) boundary layer,

$$\tau_{pl} \sim \lambda_\theta^2/\kappa. \tag{9}$$

Here we have assumed that the main mechanism for plume destruction is thermal diffusion. However, for very large Prandtl and Reynolds numbers turbulent mixing[33] may become the dominant process.

As seen from the above, the thermal BL width λ_θ plays a central role in the theory. In our previous publications[13–15] we used scaling arguments to derive this thickness. In the following section we will employ more rigorous arguments, based on similarity transformations of the underlying thermal BL equation, leading to the same result as before, and being consistent with the results in textbooks on boundary layer theory, see e.g., chapter 9 of Schlichting's textbook Ref. 29 or Ref. 34.

The plume shedding mechanism and the shedding frequency f_{shed} will be discussed in Sec. II G, together with the resulting average plume number N_{pl}^{sheet}.

D. BL thicknesses

1. Kinetic BL thickness λ_u

We recollect Prandtl's line of arguments[29,30,35] and his equation for the flow in the BL

$$u_x \partial_x u_x + u_z \partial_z u_x = \nu \partial_z^2 u_x. \tag{10}$$

We rescale with the typical velocity scale U and with the cell height L, but differently in x direction (longitudinal) and in z direction (transversal),

$$\tilde{x} = x/L, \quad \tilde{u}_x = u_x/U, \tag{11}$$

$$\tilde{z} = \sqrt{Re} z/L, \quad \tilde{u}_z = \sqrt{Re} u_z/U, \tag{12}$$

in order to achieve the parameter independent form

$$\tilde{u}_x \partial_{\tilde{x}} \tilde{u}_x + \tilde{u}_z \partial_{\tilde{z}} \tilde{u}_x = \partial_{\tilde{z}}^2 \tilde{u}_x. \tag{13}$$

Neither this equation, nor the accompanying incompressibility equation $\partial_{\tilde{x}} \tilde{u}_x + \partial_{\tilde{z}} \tilde{u}_z = 0$, nor the boundary conditions depend on the viscosity or on $Re = UL/\nu$ explicitly. Therefore also the solution to this equation cannot depend on Re and is thus universal. When Re is changed, the flow pattern undergoes a similarity transformation according to (11) for the longitudinal quantities and according to (12) for the transversal quantities. In particular, the width λ_u of the kinetic BL itself scales as

$$\lambda_u \sim L/Re^{1/2} \tag{14}$$

and the typical transversal velocity as

$$u_z \sim U/Re^{1/2}. \tag{15}$$

We note that Eq. (13) can be reduced to an ordinary differential equation (ODE) by introducing the similarity variable

$$\eta = z\sqrt{U/2\nu x} = \tilde{z}/\sqrt{2\tilde{x}} \tag{16}$$

and the stream function

$$\Psi(x,z) = \sqrt{2\nu x U} \psi(\eta), \tag{17}$$

finally leading to[29,30,35,36]

$$\psi \psi'' + \psi''' = 0 \tag{18}$$

with the boundary conditions $\psi(0) = \psi'(0) = 0$ and $\psi'(\infty) = 1$ which can be solved.[29,30,36] We stress that this reduction to an ODE is *not* necessary in order to make the statements (14) and (15) on the scaling of the kinetic BL thickness and the transversal velocity.

2. Thermal BL thickness λ_θ

Now simultaneously with Prandtl's BL equation (10) the thermal boundary layer equation

$$u_x \partial_x \theta + u_z \partial_z \theta = \kappa \partial_z^2 \theta \tag{19}$$

has to be solved. As the buoyancy term contributes only to the equation for u_z, which is not considered here, temperature is assumed to be passive. There is no room to scale the velocities differently than done in Sec. II D 1. With

Phys. Fluids, Vol. 16, No. 12, December 2004

Fluctuations in turbulent Rayleigh–Bénard convection 4465

$$\widetilde{\theta}(\eta) = \theta(x,z)/\Delta \tag{20}$$

and the similarity ansatz (16) and (17) one obtains

$$\widetilde{\theta}'' + \mathrm{Pr}\,\psi\widetilde{\theta}' = 0, \tag{21}$$

with $\psi(\eta)$ determined by Eq. (18). Equation (21) implies that the structure, thickness, and even the scaling behavior of the thermal BL depend on Pr, i.e., are nonuniversal. As shown by Pohlhausen,[34,37] Eq. (21) can be solved exactly, giving the temperature profile in the BL. In the context here only the scaling of its transversal length scale is relevant, i.e., the scaling of the thickness λ_θ of the thermal BL. It scales as[34]

$$\lambda_\theta/L \sim C(\mathrm{Pr})/\mathrm{Re}^{1/2}\mathrm{Pr}^{1/3}. \tag{22}$$

Here, $C(\mathrm{Pr})$ is an infinite alternating series given in Ref. 34. Correspondingly,

$$\mathrm{Nu} \sim \mathrm{Re}^{1/2}\mathrm{Pr}^{1/3}/C(\mathrm{Pr}). \tag{23}$$

Equation (23) holds as the thermal BL thickness is defined with the temperature gradient directly at the plates, $\partial_z\langle\theta\rangle_{A,t}(z=0) = -\Delta/(2\lambda_\theta)$. Indeed, from this definition of λ_θ and the definition of the Nusselt number

$$\mathrm{Nu} = \frac{1}{\kappa\Delta L^{-1}}[\langle u_z\theta\rangle_{A,t}(z) - \kappa\partial_z\langle\theta\rangle_{A,t}(z)] \tag{24}$$

one obtains

$$\mathrm{Nu} = \frac{L}{2\lambda_\theta}, \tag{25}$$

because $u_z(z=0)=0$.

3. Thermal BL thickness λ_θ for large Pr (upper regime)

For large $\mathrm{Pr} \gg 1$ the series for $C(\mathrm{Pr})$ converges to $C(\mathrm{Pr})=1$,[34] implying

$$\lambda_\theta \sim L/(\mathrm{Re}^{1/2}\mathrm{Pr}^{1/3}) \tag{26}$$

and

$$\mathrm{Nu} \sim \mathrm{Re}^{1/2}\mathrm{Pr}^{1/3} \tag{27}$$

in this large Pr regime.

More insight into the physics of this large (so-called upper) Pr regime, defined by the condition $\lambda_u > \lambda_\theta$, is obtained by the observation that the temperature field $\theta(x,z)$ sees a *linear* velocity profile

$$u_x(x,z) = U(x)\frac{z}{\lambda_u}, \tag{28}$$

$0 \leq z \leq \lambda_\theta$, and λ_u given by (14). Plugging this profile into the thermal BL equation (19), the similarity transformation

$$\eta = z\left(\frac{U}{\lambda_u}\right)^{1/3}(9\kappa x)^{-1/3} \tag{29}$$

allows one to reduce the thermal BL equation to an ODE, namely,

$$\widetilde{\theta}'' + 3\eta^2\widetilde{\theta}' = 0, \tag{30}$$

with the boundary conditions $\widetilde{\theta}(0)=1$ and $\widetilde{\theta}(\infty)=0$. This ODE can be solved to obtain the explicit temperature profile in the BL. From the similarity transformation (29) and the scaling of λ_u Eq. (14) one immediately gets Eq. (26) as scaling of thermal transversal lengths in this large Pr regime.

4. Thermal BL thickness λ_θ for small Pr (lower regime)

The small Pr regime (so-called lower) is defined by $\lambda_u < \lambda_\theta$. Then the z dependence of the longitudinal velocity can be neglected in the thermal BL, $u_x(x,z) \approx U(x)$. With some similarity transformation (as detailed in Ref. 29) this approximation allows to reduce the thermal BL equation (19) to the ODE

$$\widetilde{\theta}'' + 2\eta\widetilde{\theta}' = 0, \tag{31}$$

with the boundary conditions $\widetilde{\theta}(0)=1$ and $\widetilde{\theta}(\infty)=0$. It has the solution $\widetilde{\theta}(\eta)=1-\mathrm{erf}(\eta)$, giving the explicit temperature profile in the thermal BL. All scaling relations relevant in the context of this paper can already be seen from the special case $U(x) \approx U$, where the similarity transformation is particularly simple, namely

$$\eta = \frac{z}{2}\sqrt{\frac{U}{\kappa x}}. \tag{32}$$

From Eq. (32) [and from its generalization to general $U(x)$] one immediately obtains

$$\lambda_\theta \sim L/(\mathrm{Re}\,\mathrm{Pr})^{1/2} \tag{33}$$

for the scaling of thermal transversal lengths and therefore

$$\mathrm{Nu} \sim \mathrm{Re}^{1/2}\mathrm{Pr}^{1/2} \tag{34}$$

in the low Pr regime.

All relations for λ_θ and Nu of this and the preceding section are analogous to those in Chapter 9 of Schlichting's textbook (see Table 9.1 of that book) and are consistent with our earlier (less rigorous) treatment in Refs. 13–15.

E. Crossover from small to large Pr regime

The essence of the difference between the small Pr regime (lower) and large Pr regime (upper) is that in the lower regime the relevant velocity scale in the thermal BL is the large scale velocity U, whereas in the upper regime it is only $U\lambda_\theta/\lambda_u$. In Refs. 14 and 15 we have modeled the smooth transition between both with a transition function $f(x)=(1+x^4)^{-1/4}$ of the variable $x_\theta=\lambda_u/\lambda_\theta$. The relevant velocity then is $Uf(x_\theta)$, both in the lower and in the upper regime, since $f_l=f(x\to0)=1$ and $f_u=f(x\to\infty)=\lambda_\theta/\lambda_u\sim\mathrm{Pr}^{-1/3}$. Correspondingly, in the dimensionless equations of the lower regime we have to replace Re by $\mathrm{Re}f(x_\theta)$,

$$\mathrm{Re} \to \mathrm{Re}\,f(\lambda_u/\lambda_\theta), \tag{35}$$

in order to obtain expressions which hold both in the lower and in the upper regime. Indeed, it is easy to show that the replacement $\mathrm{Re} \to \mathrm{Re}\lambda_\theta/\lambda_u$ in the lower regime expressions

(33) and (34) for the thermal BL thickness and the Nusselt number, respectively, lead to the corresponding expressions (26) and (27) in the upper regime.

F. Laminarity and time dependence

The Prandtl equations (10) and (19) are time independent and therefore the resulting solutions are understood to describe laminar flow. However, evidently, high Rayleigh number thermal convection is time dependent. Therefore one wonders whether above scaling laws for λ_θ, λ_u, and Nu still hold for time-dependent flow. This is the case, provided that the viscous BL does not break down [which only happens around a BL thickness based Reynolds number between 320 (Ref. 10) and 420 (Ref. 30) and leads to the primed regimes in our phase diagram, as extensively discussed in Refs. 13–15]. Indeed, temporal changes on the time scale L/U of the wind can easily be included by adding $\partial_{\tilde{t}} \tilde{u}_x$ and $\partial_{\tilde{t}} \tilde{\theta}$, where $\tilde{t} = tU/L$, without changing the parameter independence of (13) or adding additional parameter dependences in (21). Thus the Re and Pr scaling is not changed.

Let us note that the time dependent BL equations allow for additional solutions with stronger time dependences than on the convective scale L/U. This can be attributed to the plume detachment and within our model is contained in the "background" term, which contains these intermittent breakdowns or bursts of the BL, see Sec. III A. The respective time scale is $dt \sim \lambda_\theta / u_z$ and it is shorter than L/U (if $u_z \sim U$). The corresponding strong increase of ∂_t is compensated by the term $u_z \partial_z \sim u_z / \lambda_\theta$, describing the advective change of u_x with the height z through detachment. The longitudinal advection $u_x \partial_x \sim U/L$ here is smaller by a factor $\lambda_\theta / L \sim \text{Nu}^{-1}$. Also the viscous term is small in comparison with the advective term $u_z \partial_z$, i.e., viscosity does not break the plume detachment: $\nu \partial_z^2 / u_z \partial_z \sim \nu / (U\lambda_\theta) \sim \text{Nu}/\text{Re}$ which decreases with Ra or (in the primed regimes and in IV$_l$ of our phase diagram) is at most Ra independent.

G. Number of plumes and plume shedding frequency

The number of sheet-like plumes N_{pl}^{sheet} can be estimated as follows: If we take in (7) the left-hand side (lhs) $\epsilon_{\theta,pl} \sim \kappa \Delta^2 L^{-2} \text{Nu}$, we find from Eq. (4) that $L^{-2}\text{Nu} \sim L^{-1} \lambda_\theta^{-1} N_{pl}^{sheet}$, thus $N_{pl}^{sheet} \sim (\lambda_\theta / L)\text{Nu} \sim \text{const}$, independent of Ra and Pr. The independence $N_{pl}^{sheet} \sim 1$ on Ra and Pr holds both in the lower and in the upper regime.

The same result can be obtained through physical reasoning. We assume that the thermal BL gets unstable once the Rayleigh number based on the BL thickness $\text{Ra}_{\lambda_\theta} = \beta g \Delta \lambda_\theta^3 / (\nu\kappa)$ exceeds some critical Rayleigh number for the onset of convection. Upward convection (or downward convection at the upper plate) of a fluid element in an unstable layer near Ra_c leads to the formation of convection rolls. Here, in the unstable thermal boundary layer it leads to a motion which continues into the bulk as a detaching part of the BL, i.e., as a sheet-like plume, which will be advected away by the large scale wind. The consequence of this plume separation is that the BL has locally cooled down and must warm up to the temperature difference of order Δ again. This is achieved through the heat flux $J = \text{Nu}\kappa\Delta/L$. Therefore, the

plume shedding frequency is determined by the heat flux $f_{shed} \sim J$, which has units Km/s. The relevant temperature and length scales to compensate the dimension Km are Δ and λ_θ, respectively. Therefore

$$f_{shed} \sim \frac{J}{\Delta\lambda_\theta} \sim \frac{\kappa}{L^2}\text{Nu}^2. \tag{36}$$

With Eqs. (9) and (8) we immediately obtain $N_{pl}^{sheet} \sim 1$, independent of Ra and Pr. This instability mechanism also may explain why sheet-like plumes can evolve: They result from the instability of the convection rolls in the thermal BL.

With $\text{Nu} \sim \sqrt{f\text{RePr}}$ Eq. (36) also implies

$$f_{shed} \sim Uf/L. \tag{37}$$

Indeed, Uf is the velocity seen at the edge of the thermal BL, namely, U in the lower regime and $U\lambda_\theta / \lambda_u$ in the upper regime, and therefore Eq. (37) is plausible. We also note that Eq. (37) seems to be consistent with the experimental result[38,39] for the plume shedding frequency which in fact had before been theoretically predicted.[40] The physical picture behind this theory is as follows: Hot plumes detach and are slowly advected by the large scale wind. Once they hit the upper thermal boundary layer, a fast distortion travels within the upper boundary layer, initiating a cold plume which is then slowly advected downwards, where the same mechanism is repeated.

For statistical stationarity the inverse shedding frequency f_{shed}^{-1} is proportional to the traveling time

$$\tau_{travel} \sim \frac{L}{Uf} \tag{38}$$

of (hot) plumes from the bottom to the top. Comparison with the plume lifetime τ_{pl} leads to $\tau_{pl}/\tau_{travel} \sim \tau_{pl}f_{shed} \sim 1$. This means that the (hot) plumes do reach the upper side of the cell without dissolving on their way, a result which is experimentally confirmed through visualizations in glycol (Pr $= 596$).[24]

Knowing the scaling of the number of sheet-like plumes N_{pl}^{sheet} we can now discuss the correction due to mushroom-like plumes in more detail. The thermal dissipation by mushroom-like plumes should be

$$\epsilon_{\theta,pl}^{mush} \sim \kappa \frac{\Delta^2}{\lambda_\theta^2}\left(\frac{\lambda_\theta}{L}\right)^2 N_{pl}^{mush}. \tag{39}$$

Comparison with the thermal dissipation Eq. (7) for sheet-like plumes shows that as long as N_{pl}^{mush} does not grow faster than $N_{pl}^{mush} \sim Nu$, $\epsilon_{\theta,pl}^{mush}$ is only a higher order correction to $\epsilon_{\theta,pl}^{sheet}$, which we therefore neglect. If $N_{pl}^{mush} \sim Nu$, then both contributions scale the same and again nothing would change.

H. Thermal dissipation rate due to plumes and smooth BL contributions

Summarizing all results of the last sections and plugging them into Eq. (7), one obtains the thermal dissipation rate due to the plumes and the smooth BL contributions,

$$\epsilon_{\theta,pl} \sim \kappa \frac{\Delta^2}{L^2} \, \text{Re}^{1/2} \, \text{Pr}^{1/2} \, f^{1/2}. \tag{40}$$

I. Turbulent background

The turbulent background thermal dissipation rate $\epsilon_{\theta,bg}$ originates from the large scale input, thus

$$\epsilon_{\theta,bg} \sim \frac{Uf\Delta^2}{L} \sim \kappa \frac{\Delta^2}{L^2} \, \text{Re} \, \text{Pr} \, f. \tag{41}$$

Note that as in our previous publications we have assumed that the relevant large scale time scale is $L/(Uf)$, not simply L/U. In the lower regime with $f_l = 1$ this is of course the same, but in the upper regime with $f_u = \lambda_\theta / \lambda_u$ these two scales differ. Our choice is consistent with our result for the shedding frequency (37).

J. Summary

With Eqs. (40), (41), (5), (6), (3), and (4) we thus arrive at the very same Eqs. (5) and (6) of Ref. 15 for the kinetic and thermal dissipation rate balances, respectively, but now with the refined interpretation that the first term of Eq. (6) (of Ref. 15) represents the smooth BL as well as the plume contribution (detached boundary layer) to the thermal dissipation, and the second term describes the turbulent background contribution. All numbers remain the same, and in particular the predictions for the global, external quantities Nu(Ra, Pr) (Fig. 2 of Ref. 14) and Re(Ra, Pr) (Fig. 3 of Ref. 15) and for the phase diagram (Fig. 2 of Ref. 15).

In the following we briefly summarize the agreements of our theory with experimental data for Nu(Ra, Pr) and Re(Ra, Pr). For a more detailed discussion and more references we refer to our original publications.[13–15]

The agreements are as follows.

(a) In general, there are no global power laws but only local scaling exponents.[6,9]

(b) For fixed Ra and in the low Pr regime the theory correctly gives a Nu vs Pr effective scaling exponent around 0.14 as found in various experiments and simulations.[19,41–43]

(c) For large Pr the curve Nu (Pr) saturates and even slightly decreases.[11] Even the absolute numbers very nicely agree with our predictions made prior to the experiment.

(d) For fixed Pr and Ra up to 10^{11} the various measurements made for Nu(Ra) can be accounted for within our theory. For small $\text{Pr} \ll 1$ the effective exponent is close to 0.25,[41] for large $\text{Pr} \approx 1–7$ it is around 0.29.[3,7,9,10,28,44–46]

(e) Beyond Ra$=10^{11}$ our theory is consistent with the Oregon measurements on Nu vs Ra,[9] not with the Grenoble data.[7,8,47,48] However, a transition towards a steeper effective exponent closer to $1/2$ can be explained by the instability of the kinetic BL to be expected around Ra$\approx 10^{15}$.[15] This instability, however, should first arise in the Oregon data as those achive higher Ra.

(f) Once the thermal and kinetic boundary layers are eliminated in numerical simulations and replaced by periodic boundary conditions, the ultimate scaling regime with Nu $\sim$ Ra$^{1/2}$ shows up,[49] as predicted by our unifying theory.

Note that the numerical simulations of this so-called "homogeneous Rayleigh–Bénard turbulence"[49,50] are also consistent with the Prandtl number dependence in this ultimate regime (regime IV$_l$ in the phase diagram of Refs. 13–15), namely, Nu $\sim$ Ra$^{1/2}$ Pr$^{1/2}$ and Re $\sim$ Ra$^{1/2}$ Pr$^{-1/2}$.

(g) The effective Re vs Ra scaling exponent (for fixed Pr=5.5) is around 0.45.[12,39,51,52]

(h) The local scaling of Re vs Pr shows two regimes: For fixed Ra$=10^6$ the small-Pr effective exponent is -0.60 and the large-Pr effective exponent -1.0, see Fig. 3(b) of Ref. 15. The numerical results obtained two years later for the respective exponents are -0.607 ± 0.013 and -0.998 ± 0.014.[19] In both theory and numerics the crossover is around Pr≈ 1. The experimental result by Lam *et al.*[12] is Re(Pr) $\sim$ Pr$^{-0.95}$ for Pr between 6 and 1400.

The major disagreement of our theory with experiment is on the thickness of the kinetic BL at the top and bottom plates which scales as $\lambda_u / L \sim$ Ra$^{-0.16}$,[12,53,54] much weaker than suggested by the theory $\lambda_u / L \sim$ Ra$^{-0.23}$. However, the sidewall scaling of the kinetic BL thickness found in those papers does agree with theoretical prediction. A possible solution of this problem has been suggested by us in Ref. 4.

III. HEAT FLUX

A. Global heat flux

Hitherto, the core of our argument has been based on the dissipation rates, and not on the heat flux Eq. (24). From our point of view this approach is the easier one, as the thermal dissipation rate is a quantity *quadratic* in θ (or, to be precise, in $\partial_i \theta$), whereas in Eq. (24) θ enters linearly, and statements on correlations are necessary. However, the thermal dissipation rate ϵ_θ is intimately related to the heat flux Nu via the exact Eq. (4), $\epsilon_\theta / (\kappa \Delta^2 / L^2) = $ Nu. This is a remarkable relation, as on the left-hand side we have a *volume average*, whereas on the right-hand side we have a flux, *averaged over the cross-section* of the cell at *any* arbitrary height z,

$$\frac{\epsilon_\theta}{\kappa \Delta^2 L^{-2}} = \text{Nu} = \frac{1}{\kappa \Delta L^{-1}} [\langle u_z \theta \rangle_{A,t}(z) - \kappa \partial_z \langle \theta \rangle_{A,t}(z)]. \tag{42}$$

The average $\langle \cdots \rangle_{A,t}(z)$ is taken over the *full* area parallel to the ground at height z and over time. Clearly, the turbulent background and the plume contributions to ϵ_θ with their different scaling behaviors $\epsilon_{\theta,bg}/(\kappa \Delta^2 / L^2) \sim f \, \text{Re} \, \text{Pr}$ and $\epsilon_{\theta,pl}/(\kappa \Delta^2 / L^2) \sim f^{1/2} \, \text{Re}^{1/2} \, \text{Pr}^{1/2}$ must be present also on the right-hand side of Eq. (42). This must hold for *any* height z, since the heat current, i.e., the right-hand side (rhs), is independent of z. This, in particular, means that there must be turbulent background contributions to the heat flux $\sim f \, \text{Re} \, \text{Pr}$ already for very small z in the boundary layer and vice versa plume contributions $\sim f^{1/2} \, \text{Re}^{1/2} \, \text{Pr}^{1/2}$ at any height z. Figure 2 of Ref. 24 suggests that for $z \approx L/2$ at least for glycol (Pr≈ 596) the plume contributions are concentrated close to the sidewall boundaries and the background contributions are more in the center of the cell. In any case, we know that for any height z from the two terms in Eq. (42) there can only be contributions $\sim f \, \text{Re} \, \text{Pr}$ and $\sim f^{1/2} \, \text{Re}^{1/2} \, \text{Pr}^{1/2}$ to the dimensionless heat flux (Nusselt number), but those contributions

even *must* be there. Realizing this, it is by the way not surprising that the ratio of the thermal dissipation rate in the plate boundary layers and the thermal dissipation rate in a region with z outside the plate boundary layers is constant, i.e., independent of Ra, as found in Ref. 16: For any plane with constant z *both* contributions $\sim f^{1/2}\,\mathrm{Re}^{1/2}\,\mathrm{Pr}^{1/2}$ and $\sim f\,\mathrm{Re}\,\mathrm{Pr}$, originating from plumes and background, respectively, must contribute, and always in the same ratio.

This argument supports our earlier ansatz (7) on the dimensionality of the plumes relevant for the thermal dissipation, namely, that they are sheet-like rather than mushroom-like. Indeed, for very small z the dimensionality of the thermal structure is out of question: It is the two-dimensional thermal BL itself. Due to the z independence of above ratio, also the relevant thermal structures for larger z must be two-dimensional, i.e., sheet-like rather than mushroom-like. The prediction of our theory, therefore, is that at any height z sheet-like thermal structures exist (or at least decayed sheet-like thermal structures).

Let us now have a more detailed look at relation (42) for various heights z. For $z=0$ we had done so already in Sec. II D 2. The first term on the rhs of Eq. (42) vanishes as $u_z(z=0)=0$ and the second term gives $L/(2\lambda_\theta)$, resulting in the known relation (25) between Nu and λ_θ.

For nonzero z but z still within the boundary layer we estimate

$$\frac{-\kappa\partial_z\langle\theta\rangle_{A,t}(z\in\mathrm{BL})}{\kappa\Delta L^{-1}}\sim\frac{L}{\lambda_\theta}\sim f^{1/2}\,\mathrm{Re}^{1/2}\,\mathrm{Pr}^{1/2}. \tag{43}$$

This relation not only follows from the estimate, but more rigorously from relations (34) and (27), under the assumption that the Prandtl type analysis of chapter II is applicable to at least the smooth parts of the thermal BL. The same argument applies to the smooth, plume-like part of the other term $\sim\langle u_z\theta\rangle_{A,t}(z)/(\kappa\Delta L^{-1})$, for which we split the area average $\langle\cdots\rangle_{A,t}(z)$ into an average over the turbulent background or intermittent burst regions across the layer A and an average over the plumes' and smooth BL parts' regions,

$$\langle\cdots\rangle_{A,t}(z)=\langle\cdots\rangle_{\{x,y\}\in bg,t}(z)+\langle\cdots\rangle_{\{x,y\}\in pl,t}(z). \tag{44}$$

For example, for the plume and smooth BL contributions we have to conclude that

$$\frac{\langle u_z\theta\rangle_{\{x,y\}\in pl,t}(z\in\mathrm{BL})}{\kappa\Delta L^{-1}}\sim f^{1/2}\,\mathrm{Re}^{1/2}\,\mathrm{Pr}^{1/2}, \tag{45}$$

also due to Eqs. (34) and (27). For small degree of turbulence this is the dominant contribution, but for increasing Ra the thermal BL will more and more often become unstable, leading to intermittent bursts, which form kind of a turbulent background. The heat flux associated with these events must scale as

$$\frac{\langle u_z\theta\rangle_{\{x,y\}\in bg,t}(z\in\mathrm{BL})}{\kappa\Delta L^{-1}}\sim\frac{fU\Delta}{\kappa\Delta L^{-1}}\sim f\,\mathrm{Re}\,\mathrm{Pr}. \tag{46}$$

Note that for the estimate of these turbulent background bursts we use the *longitudinal* velocity fU felt at the edge of the thermal BL. We consider this as more appropriate than to use the transversal velocity (15), as it originates from the

Prandtl type similarity analysis which is not applicable for the turbulent bursts, but only for the smooth parts of the BL.

For heights in the middle of the cell (say, $z\approx L/2$) the second term $\sim\partial_z\langle\theta\rangle_{A,t}(z)$ in Eq. (42) does not contribute as the mean temperature in the center is about constant. The first term $\sim\langle u_z\theta\rangle_{A,t}(z)$ again must have two contributions, one corresponding to the plumes with the smooth BL type scaling

$$\frac{\langle u_z\theta\rangle_{\{x,y\}\in pl,t}(z\approx L/2)}{\kappa\Delta L^{-1}}\sim f^{1/2}\,\mathrm{Re}^{1/2}\,\mathrm{Pr}^{1/2}, \tag{47}$$

and one corresponding to the turbulent background

$$\frac{\langle u_z\theta\rangle_{\{x,y\}\in bg,t}(z\approx L/2)}{\kappa\Delta L^{-1}}\sim\frac{fU\Delta}{\kappa\Delta L^{-1}}\sim f\,\mathrm{Re}\,\mathrm{Pr}. \tag{48}$$

One expects that the $\{x,y\}\in pl$ are preferably near the sidewall, while $\{x,y\}\in bg$ will predominantly be in the center region.

B. Local heat fluxes

Global heat flux measurements can of course only give the *sum* of plume and turbulent background contributions. However, in local simultaneous measurements of the vertical velocity and the temperature it may be possible to disentangle plume and turbulent background contributions. Indeed, in a recent paper Ching et al.[21] offer an algorithm to detect plumes in time series of the vertical velocity and the temperature. If the heat transfer associated with the plumes and with the background can be calculated from that algorithm, it will be possible to check the predictions (47) and (48) on the respective scaling behavior.

For the time being we must make use of the experimental observation[24] that for $z\approx L/2$ and close to the sidewall the flow is dominated by plumes, whereas in the center the turbulent background fluctuations dominate the flow, and plumes only occur occasionally. Therefore we predict that the local heat flux close to the wall should scale more like (47), whereas the local heat flux in the center should scale more like (48),

$$\mathrm{Nu(sidewall)}\sim f^{1/2}\,\mathrm{Re}^{1/2}\,\mathrm{Pr}^{1/2}, \tag{49}$$

$$\mathrm{Nu(center)}\sim f\,\mathrm{Re}\,\mathrm{Pr}. \tag{50}$$

The two scaling relations are shown in Figs. 1 and 2. For Nu(sidewall) the local slope in the low Ra regime is around 0.22 for all Pr. This value is very similar to what has been found by Tong and collaborators for the measurements of the local Nusselt number close to the sidewall, in experiments in water with Ra up to 10^{10} (Tong, private communication). In the center of the cell Tong and collaborators found a much steeper local slope in that Ra regime. Our theoretical result of a slope around 0.44 for Nu(center) and Pr=5.5 is clearly consistent with their measurement. Note that for small Ra the absolute values of Nu(center) are of course much smaller than those for Nu(sidewall), as in that small Ra regime most of the heat is transported by the large scale wind.[24] Only for much larger Ra the heat flux through the center takes over.
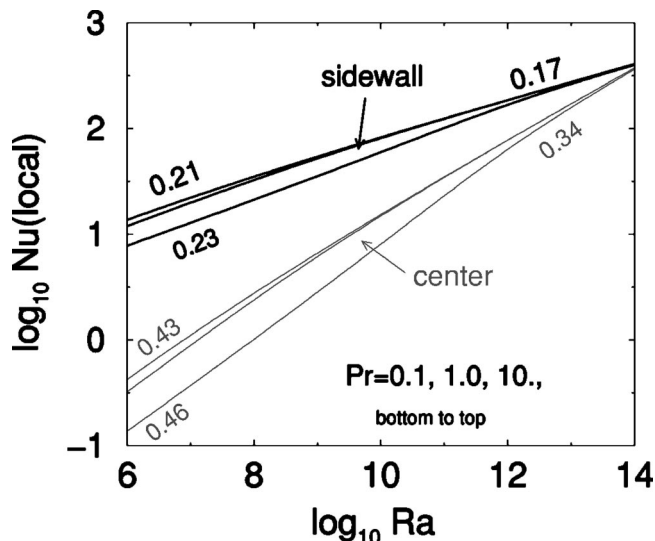
FIG. 1. Nu(sidewall) (solid black lines) and Nu(center) (gray lines) as functions of Ra for Pr$=10^{-1}$, 10^0, and 10^1, bottom to top. The local slopes for Nu(sidewall) typically vary between 0.21 and 0.17 for Pr$=10$ and 0.23 and 0.17 for Pr$=10^{-1}$. The local slopes for Nu(center) typically vary between 0.43 and 0.34 for Pr$=10$ and 0.46 and 0.34 for Pr$=10^{-1}$.

The experiments by Tong and collaborators suggest that this would be the case at Ra$=10^{14}$.

In the high Ra regime the local scaling exponents of Nu(local) vs Ra are around 0.17 for Nu(sidewall) and 0.34 for Nu(center), respectively. For fixed Rayleigh numbers between 10^8 and 10^{11} the local slopes of Nu(local) as function of Pr are as follows: For Nu(sidewall) around 0.22 for small Pr and around -0.04 for large Pr and for Nu(center) around 0.45 for small Pr and around -0.05 for large Pr, see Fig. 2. To our knowledge none of these exponents has been measured up to now. Note again that these values only hold once
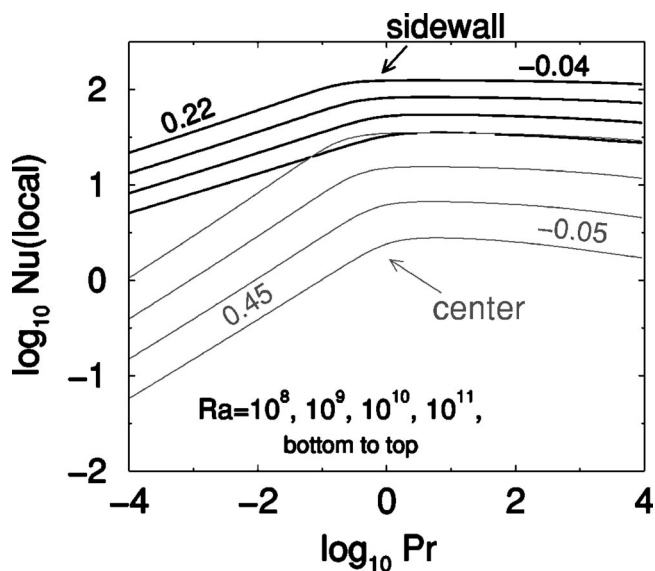

FIG. 2. Nu(sidewall) (solid black lines) and Nu(center) (gray lines) as functions of Pr for Ra$=10^8$, 10^9, 10^{10}, and 10^{11}, bottom to top. For Nu(sidewall) the local slopes in the small Pr regime are around 0.22 and those in the large Pr regime around -0.04. For Nu(center) the local slopes in the small Pr regime are around 0.45 and those in the large Pr regime around -0.05.

one succeeds to fully separate the heat flux due to the plumes and the heat flux due to the turbulent background.

That the splitting of the cell into sidewall and center regions is not unreasonable is also supported by the recent results of Xia and collaborators[55] who found that the rotation frequencies of the inner core and of the outer large scale wind show different scaling with Ra, namely, $\sim \kappa L^{-2} Ra^{0.4}$ and $\sim \kappa L^{-2} Ra^{0.5}$, respectively.

C. Temperature-velocity correlations in the plume dominated regime

There is an interesting corollary from Eq. (47) for the heat transport in the plume dominated regime. The relation suggests that in that regime the correlation between temperature and vertical velocity scales as

$$\frac{\langle u_z \theta \rangle_{\{x,y\} \in pl, t}}{\langle u_z \rangle_{\{x,y\} \in pl, t} \langle \theta \rangle_{\{x,y\} \in pl, t}} \left(z \approx \frac{L}{2} \right) \sim \frac{\kappa \Delta L^{-1} \sqrt{f \, Re \, Pr}}{U \Delta} \sim \frac{f}{Nu},$$

(51)

i.e., like $1/Nu$ in the lower regime and like $Pr^{-1/3}/Nu$ in the upper regime. Here we have assumed that at midheight the typical upwards plume velocity $\langle u_z \rangle_{\{x,y\} \in pl, t} \sim U$ and Nu $\sim \sqrt{f Re Pr}$. Physically, indeed the result (51) makes sense as one expects that the correlation between temperature and upwards velocity gets weaker with increasing Nu, due to the increasing degree of turbulence. The prediction (51) for the plume dominated regime is open to experimental validation. One could, e.g., measure the temperature-velocity correlation close to the sidewalls where the plume density is particularly high.[24]

IV. FLUCTUATIONS

A. Temperature fluctuations

The results from our unifying scaling theory for ϵ_θ and thus Nu can also be used to make predictions on the scaling of the fluctuations. The total thermal dissipation rate Eq. (1) has two contributions with different Re and Pr scaling, namely, turbulent background and plumes, Eqs. (41) and (40). The same should hold for the temperature fluctuations (2). Both the (square of the) temperature fluctuations and the thermal dissipation rates are *additive*. The background thermal dissipation rate corresponds to the background thermal fluctuations θ'_{bg},

$$\epsilon_{\theta, bg} \sim \kappa \frac{\Delta^2}{L^2} \, Re \, Pr \, f \sim \kappa \frac{(\theta'_{bg})^2}{\eta_\theta^2},$$

(52)

where $\eta_\theta = \kappa^{3/4} / \epsilon_u^{1/4} = Pr^{-3/4} \eta$ is the inner thermal length scale, which scales as $\eta_\theta \sim L Pr^{-3/4} Re^{-3/4}$, due to $\epsilon_u \sim U^3 / L$. Here, $\eta \sim L Re^{-3/4}$ is the Kolmogorov length. From Eq. (52) one immediately obtains

$$\frac{\theta'_{bg}}{\Delta} \sim Pr^{-1/4} \, Re^{-1/4} f^{1/2}.$$

(53)

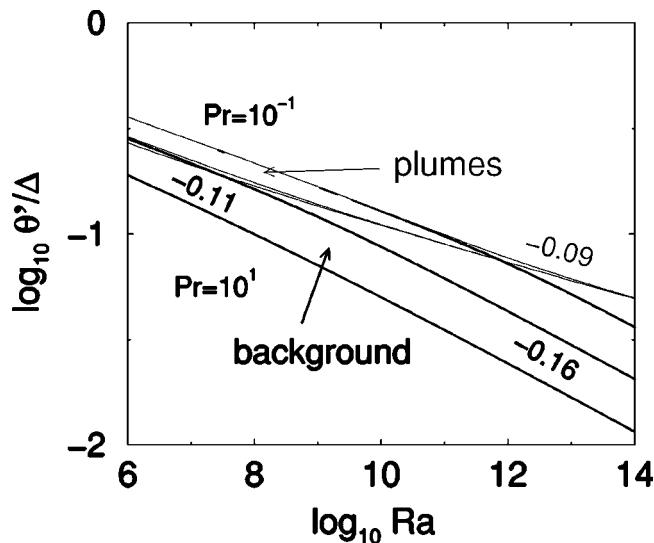For the plume thermal fluctuations θ'_{pl} it must hold

FIG. 3. θ'_{bg}/Δ (solid black lines) and θ'_{pl}/Δ (gray lines) as functions of Ra for $\mathrm{Pr}=10^{-1}$, 10^0, and 10^1, top to bottom. For θ'_{bg}/Δ the local slopes typically vary between -0.13 and -0.16 for $\mathrm{Pr}=10$ and -0.11 and -0.16 for $\mathrm{Pr}=10^{-1}$. For θ'_{pl}/Δ the local slopes typically vary between -0.11 and -0.09 for all given Pr.

FIG. 4. θ'_{bg}/Δ (solid black lines) and θ'_{pl}/Δ (gray lines) as functions of Pr for $\mathrm{Ra}=10^8$, 10^9, 10^{10}, and 10^{11}, top to bottom. For θ'_{bg}/Δ the local slope in the large Pr regime is about -0.24, that one in the small Pr regime about -0.11. For θ'_{pl}/Δ the local slope in the small Pr regime is also about -0.11, that one in the large Pr regime about 0.01.

$$\epsilon_{\theta,pl} \sim \kappa \frac{\Delta^2}{L^2} \,\mathrm{Re}^{1/2}\,\mathrm{Pr}^{1/2} f^{1/2} \sim \kappa \frac{(\theta'_{pl})^2}{\lambda_\theta^2}. \tag{54}$$

Here we have used λ_θ as the typical length scale of the plumes. Using $L/\lambda_\theta \sim f^{1/2}\mathrm{Re}^{1/2}\mathrm{Pr}^{1/2}$ as above for the (inverse) thickness of the detached thermal boundary layer we obtain

$$\frac{\theta'_{pl}}{\Delta} \sim f^{-1/4}\,\mathrm{Re}^{-1/4}\,\mathrm{Pr}^{-1/4}, \tag{55}$$

which for small Pr, where $\lambda_u < \lambda_\theta$ and thus $f=1$, interestingly has the same scaling as for the background thermal fluctuations. In general, the thermal background and plume fluctuations add according to Eq. (2). The relative weight of the background and the plumes may vary depending on the exact position in the cell: Close to the sidewalls the plumes may dominate; in the center the background may dominate.

In Figs. 3 and 4 we show the temperature fluctuations as function of Ra and Pr. These results are based on Re (Ra, Pr) and Nu (Ra, Pr) as produced by our unifying theory.[14,15] The resulting dependence of θ'/Δ on Ra (Fig. 3) with a local slope between -0.11 and -0.16 seems to be consistent with the experimental results. For example, Daya and Ecke[25,26] measure $\theta'/\Delta \sim \mathrm{Ra}^{-0.10\pm0.02}$ in water; Niemela et al.[9] get $\theta'/\Delta \sim \mathrm{Ra}^{-0.145}$ in helium gas; Castaing et al.[28] get $\theta'/\Delta \sim \mathrm{Ra}^{-1/7}$, also in helium gas.

The resulting dependence of θ'/Δ on Pr (Fig. 4) reveals local scaling exponents of around -0.11 for both θ'_{bg}/Δ and θ'_{pl}/Δ in the low Pr regime. In the large Pr regime we have a local slope of about $+0.01$ for θ'_{pl}/Δ and of about -0.24 for θ'_{bg}/Δ. All these dependences are much weaker than the exponent -0.38 ± 0.04 which had been found in the experiments by Daya and Ecke[26] for (large) Pr between 2 and 12. We have no explanation for this discrepancy. It will remain the only one with experiment. In view of this discrepancy and in
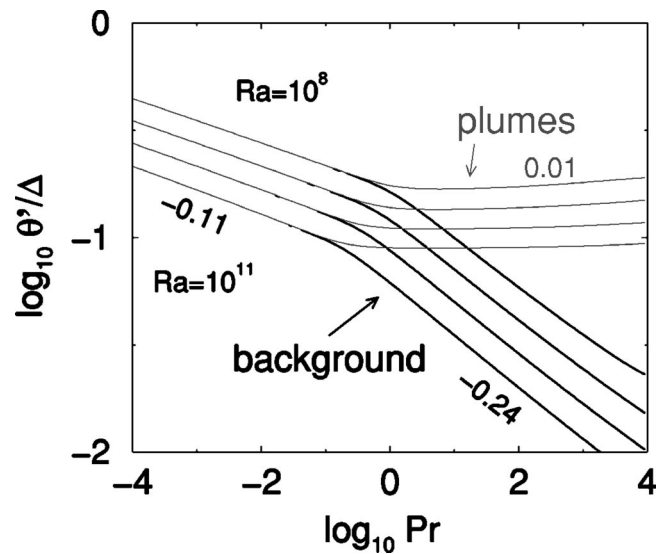
view of the large difference in the local scaling exponents for θ'_{pl}/Δ and for θ'_{bg}/Δ we consider new measurements of the Pr dependence of the temperature fluctuations at various locations in the cell as worthwhile.

B. Velocity fluctuations

The (bulk) velocity fluctuations u' are estimated within the same spirit and as in Ref. 15, namely,

$$\epsilon_{u,bulk} \sim \frac{U^3}{L} \sim \nu \frac{(u')^2}{\eta^2}, \tag{56}$$

resulting in

$$\frac{u'}{U} = \frac{\mathrm{Re}'}{\mathrm{Re}} \sim \mathrm{Re}^{-1/4}. \tag{57}$$

The dependence of Re'/Re on Ra and Pr is shown in Figs. 5 and 6. The local exponent of Re'/Re vs Ra is -0.11 for all shown Pr numbers. The local exponent of Re'/Re vs Pr is between 0.17 and 0.21 for the Ra shown in Fig. 6, with a tendency to be slightly larger in the large Pr regime. From Figs. 4(a) and 3(b) of Ref. 15 we extract a local scaling law $\mathrm{Re}\sim\mathrm{Ra}^{0.45}\mathrm{Pr}^{-1.0}$ for Ra around 10^9–10^{10} and Pr around 2–12 where the experiments by Daya and Ecke took place.[26] Using these values we obtain from their given local scaling exponents for Re' the following: $\mathrm{Re}'/\mathrm{Re}\sim\mathrm{Ra}^\lambda\mathrm{Pr}^\omega$ with λ between 0.05 and 0.01 and $\omega=0.20\pm0.03$. While the Pr exponent seems to be in very nice agreement, the Ra exponent λ even seems to have a different sign than in experiment. However, already in chapter 5 of Ref. 4 we had mentioned that in fact it is consistent with the experimental results in Refs. 12, 25, and 26. Moreover, other researchers (Ref. 56) had given λ values between -0.02 and -0.11, though for a square cell. Clearly, more experimental data are needed also for the relative velocity fluctuations.
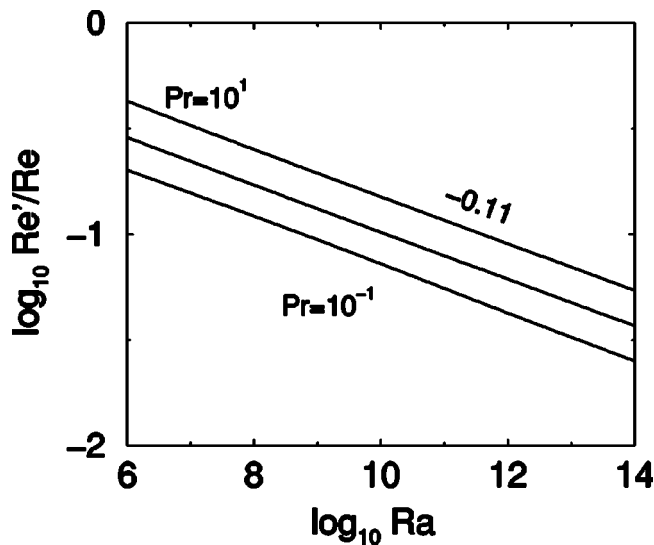
FIG. 5. $u'/U = \mathrm{Re}'/\mathrm{Re}$ as function of Ra for $\mathrm{Pr}=10^{-1}$, 10^0, and 10^1, bottom to top. The local slopes are around -0.11.

V. CONCLUSIONS AND SUGGESTION FOR MEASUREMENTS

The central idea of this paper was to split the thermal dissipation rate and the thermal fluctuations into a background contribution and a plume contribution. Though from flow visualization it is easy to visually identify "plumes," it is by far nontrivial to disentangle temperature signals into plume and nonplume contributions, though first attempts have already been made.[19,21] What may be easier is to identify "large plumes." For those clearly the predicted scaling $\epsilon_{\theta,pl}/(\kappa\Delta^2/L^2) \sim \mathrm{Re}^{1/2}\mathrm{Pr}^{1/2}f^{1/2}$ should hold, whereas the turbulent background, which should scale like $\epsilon_{\theta,bg}/(\kappa\Delta^2/L^2) \sim \mathrm{RePr}f$, may be contaminated by the contributions from "small plumes." Pattern recognition methods used for hot-
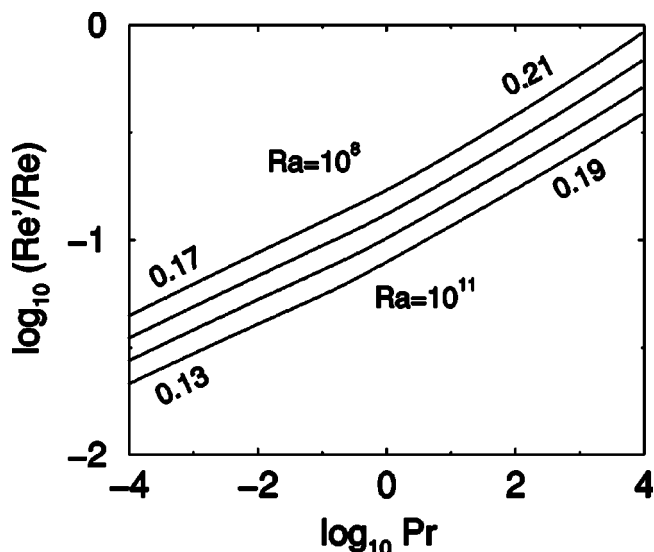

FIG. 6. $u'/U = \mathrm{Re}'/\mathrm{Re}$ as function of Pr for Ra$=10^8$, 10^9, 10^{10}, and 10^{11}, top to bottom. The local slopes vary between 0.17 and 0.21 for Ra$=10^8$ and 0.13 and 0.19 for Ra$=10^{11}$.

wire signals in bubbly flow[57] in order to identify bubbles touching the hot wire may be useful for further plume identifications.

We close the paper with a list of detailed predictions following from our theory, which should be checked against experimental and numerical observations.

(i) The area averaged thermal dissipation rate should be the same in any plane (of some small width) with given fixed distance z from the ground, just as the total area average Nu(z), which should be independent of height z, due to heat flux conservation.

(ii) A consequence of this statement is that at any height z *sheet-like* (i.e., two-dimensional) thermal structures should exist (or at least decayed sheet-like thermal structures) and dominate the thermal dissipation of the plume part, just as assumed in our ansatz (7). Three-dimensional flow visualizations will be necessary to check this prediction.

(iii) The number of sheet-like plumes N_{pl}^{sheet} is constant, independent of Ra and Pr. In case of mushroom-like plumes their number N_{pl}^{mush} does not increase stronger than $\sim$Nu. If they developed from the decay of sheet-like plumes, their number would scale as $\sim L/\lambda_\theta \sim$ Nu, satisfying this upper threshold.

(iv) For large Pr, when the flow is organized in a convection role, the thermal dissipation rate should peak close to the sidewalls as there it is dominated by the plumes.

(v) The plume-dominated part of the thermal dissipation should scale as $\epsilon_{\theta,pl}/(\kappa\Delta^2/L^2) \sim (\mathrm{RePr}f)^{1/2}$, with $f \sim 1$ in the lower regime and $f \sim \mathrm{Pr}^{-1/3}$ in the upper regime.

(vi) The background-dominated part of the thermal dissipation should scale as $\epsilon_{\theta,pl}/(\kappa\Delta^2/L^2) \sim \mathrm{RePr}f$.

(vii) The thermal fluctuations should scale according to Figs. 3 and 4.

(viii) In particular, the Pr dependence of the temperature fluctuations close to the sidewall, where the plumes dominate, should be *weaker* than in the center of the flow.

(ix) The velocity fluctuations should scale according to Figs. 5 and 6.

(x) In the plume-dominated regime the normalized correlation $\langle u_z\theta\rangle/(\langle u_z\rangle\langle\theta\rangle)$ scales like $\sim 1/$Nu in the lower regime and like $\sim \mathrm{Pr}^{-1/3}/$Nu in the upper regime.

(xi) Perhaps the most important and interesting prediction is that the *local* heat flux should show a stronger Ra dependence in the turbulent background fluctuation dominated center of the cell than close to the plume-dominated sidewalls. If one succeeds in a full separation of the heat flux into a contribution due to plumes and one due to the turbulent background fluctuations, the repective scaling should be as shown in Figs. 1 and 2.

ACKNOWLEDGMENTS

[1] L. P. Kadanoff, "Turbulent heat flow: Structures and scaling," Phys. Today **54** (8), 34 (2001).

[2] G. Ahlers, S. Grossmann, and D. Lohse, "Hochpräzision im Kochtopf: Neues zur turbulenten Konvektion," Physik Journal **1** (2), 31 (2002).

[3] E. D. Siggia, "High Rayleigh number convection," Annu. Rev. Fluid Mech. **26**, 137 (1994).

[4] S. Grossmann and D. Lohse, "On geometry effects in Rayleigh–Bénard convection," J. Fluid Mech. **486**, 105 (2003).

[5] X. Xu, K. M. S. Bajaj, and G. Ahlers, "Heat transport in turbulent Rayleigh–Bénard convection," Phys. Rev. Lett. **84**, 4357 (2000).

[6] G. Ahlers and X. Xu, "Prandtl-number dependence of heat transport in turbulent Rayleigh–Bénard convection," Phys. Rev. Lett. **86**, 3320 (2001).

[7] X. Chavanne, F. Chilla, B. Castaing, B. Hebral, B. Chabaud, and J. Chaussy, "Observation of the ultimate regime in Rayleigh–Bénard convection," Phys. Rev. Lett. **79**, 3648 (1997).

[8] X. Chavanne, F. Chilla, B. Castaing, B. Chabaud, and B. Hebral, "Turbulent Rayleigh–Bénard convection in gaseous and liquid He," Phys. Fluids **13**, 1300 (2001).

[9] J. Niemela, L. Skrebek, K. R. Sreenivasan, and R. Donnelly, "Turbulent convection at very high Rayleigh numbers," Nature (London) **404**, 837 (2000).

[10] J. Niemela and K. R. Sreenivasan, "Confined turbulent convection," J. Fluid Mech. **481**, 355 (2003).

[11] K.-Q. Xia, S. Lam, and S. Q. Zhou, "Heat-flux measurement in high-Prandtl-number turbulent Rayleigh–Bénard convection," Phys. Rev. Lett. **88**, 064501 (2002).

[12] S. Lam, X. D. Shang, S. Q. Zhou, and K.-Q. Xia, "Prandtl-number dependence of the viscous boundary layer and the Reynolds-number in Rayleigh–Bénard convection," Phys. Rev. E **65**, 066306 (2002).

[13] S. Grossmann and D. Lohse, "Scaling in thermal convection: A unifying view," J. Fluid Mech. **407**, 27 (2000).

[14] S. Grossmann and D. Lohse, "Thermal convection for large Prandtl number," Phys. Rev. Lett. **86**, 3316 (2001).

[15] S. Grossmann and D. Lohse, "Prandtl and Rayleigh number dependence of the Reynolds number in turbulent thermal convection," Phys. Rev. E **66**, 016305 (2002).

[16] R. Verzicco and R. Camussi, "Numerical experiments on strongly turbulent thermal convection in a slender cylindrical cell," J. Fluid Mech. **477**, 19 (2003).

[17] R. Verzicco, "Turbulent thermal convection in a closed domain: Viscous boundary layer and mean flow effects," Eur. Phys. J. B **35**, 133 (2003).

[18] D. Funfschilling and G. Ahlers, "Plume motion and large scale circulation in a cylindrical Rayleigh–Bénard cell," Phys. Rev. Lett. **92**, 194502 (2004).

[19] M. Breuer, S. Wessling, J. Schmalzl, and U. Hansen, "Effect of inertia in Rayleigh–Bénard convection," Phys. Rev. E **69**, 026302 (2004).

[20] E. Bodenschatz, W. Pesch, and G. Ahlers, "Recent developments in Rayleigh–Bénard convection," Annu. Rev. Fluid Mech. **32**, 709 (2000).

[21] E. S. C. Ching, H. Guo, X. D. Shang, P. Tong, and K.-Q. Xia, "Extraction of plumes in turbulent thermal convection," Phys. Rev. Lett. **93**, 124501 (2004).

[22] A. Berschadskii, J. J. Niemela, A. Praskovsky, and K. R. Sreenivasan, "Clusterization and intermittency of temperature fluctuations in turbulent convection" Phys. Rev. E **69**, 056314 (2004).

[23] S. Wunsch and A. R. Kersten, "A stochastic model for high Rayleigh number convection," J. Fluid Mech. (to be published).

[24] X. D. Shang, X. L. Qiu, P. Tong, and K. Q. Xia, "Measured local heat transport in turbulent Rayleigh–Bénard convection," Phys. Rev. Lett. **90**, 074501 (2003).

[25] Z. A. Daya and R. E. Ecke, "Does turbulent convection feel the shape of the container?" Phys. Rev. Lett. **87**, 184501 (2001).

[26] Z. A. Daya and R. E. Ecke, "Prandtl number dependence of interior temperature and velocity fluctuations in turbulent convection," Phys. Rev. E **66**, 045301 (2002).

[27] G. Zocchi, E. Moses, and A. Libchaber, "Coherent structures in turbulent convection: An experimental study," Physica A **166**, 387 (1990).

[28] B. Castaing, G. Gunaratne, F. Heslot, L. Kadanoff, A. Libchaber, S. Thomae, X. Z. Wu, S. Zaleski, and G. Zanetti, "Scaling of hard thermal turbulence in Rayleigh–Bénard convection," J. Fluid Mech. **204**, 1 (1989).

[29] H. Schlichting and K. Gersten, *Boundary Layer Theory*, 8th ed. (Springer, Berlin, 2000).

[30] L. D. Landau and E. M. Lifshitz, *Fluid Mechanics* (Pergamon, Oxford, 1987).

[31] H. D. Xi, S. Lam, and K.-Q. Xia, "From laminar plumes to organized flows: The onset of large-scale circulation in turbulent thermal convection," J. Fluid Mech. **503**, 47 (2004).

[32] S. Q. Zhou and K.-Q. Xia, "Plume statistics in thermal turbulence: Mixing of an active scalar," Phys. Rev. Lett. **89**, 184502 (2002).

[33] E. Villermaux and J. Duplat, "Mixing as an aggregation process," Phys. Rev. Lett. **91**, 184501 (2003).

[34] D. Meksyn, *New Methods in Laminar Boundary Layer Theory* (Pergamon, Oxford, 1961).

[35] L. Prandtl, in *Über Flüssigkeitsbewegung bei sehr kleiner Reibung*, in Verhandlungen des III. Int. Math. Kongr., Heidelberg, 1904 (Teubner, Leipzig, 1905), pp. 484–491.

[36] H. Blasius, "Grenzschichten in Flüssigkeiten mit kleiner Reibung," Z. Math. Phys. **56**, 1 (1908).

[37] E. Pohlhausen, "Zur nährungsweisen Integration der Differentialgleichung der laminaren Grenzschicht," Z. Angew. Math. Mech. **1**, 252 (1921).

[38] X. L. Qiu and P. Tong, "Large-scale coherent rotation and oscillation in turbulent thermal convection," Phys. Rev. E **61**, R6075 (2000).

[39] X. L. Qiu and P. Tong, "Onset of coherent oscillations in turbulent Rayleigh–Bénard convection," Phys. Rev. Lett. **87**, 094501 (2001).

[40] E. Villermaux, "Memory-induced low frequency oscillations in closed convection boxes," Phys. Rev. Lett. **75**, 4618 (1995).

[41] S. Cioni, S. Ciliberto, and J. Sommeria, "Strongly turbulent Rayleigh–Bénard convection in mercury: Comparison with results at moderate Prandtl number," J. Fluid Mech. **335**, 111 (1997).

[42] R. Verzicco and R. Camussi, "Prandtl number effects in convective turbulence," J. Fluid Mech. **383**, 55 (1999).

[43] R. Kerr and J. R. Herring, "Prandtl number dependence of Nusselt number in direct numerical simulations," J. Fluid Mech. **419**, 325 (2000).

[44] F. Heslot, B. Castaing, and A. Libchaber, "Transition to turbulence in helium gas," Phys. Rev. A **36**, 5870 (1987).

[45] Y. Shen, P. Tong, and K.-Q. Xia, "Turbulent convection over rough surfaces," Phys. Rev. Lett. **76**, 908 (1996).

[46] P. E. Roche, B. Castaing, B. Chabaud, and B. Hebral, "Heat transfer in turbulent Rayleigh–Bénard convection below the ultimate regime," J. Low Temp. Phys. **134**, 1011 (2004).

[47] P. E. Roche, B. Castaing, B. Chabaud, and B. Hebral, "Observation of the 1/2 power law in Rayleigh–Bénard convection," Phys. Rev. E **63**, 045303 (2001).

[48] P. E. Roche, B. Castaing, B. Chabaud, and B. Hebral, "Prandtl and Rayleigh numbers dependences in Rayleigh–Bénard convection," Europhys. Lett. **58**, 693 (2002).

[49] D. Lohse and F. Toschi, "The ultimate state of thermal convection," Phys. Rev. Lett. **90**, 034502 (2003).

[50] E. Calzavarini, F. Toschi, and R. Tripiccione, in *Advances in Turbulence X*, edited by H. I. Andersson and P. A. Krogstad (International Center for Numerical Methods in Engineering, CIMNE, Barcelona, 2004), p. 121.

[51] X. L. Qiu and P. Tong, "Large scale velocity structures in turbulent thermal convection," Phys. Rev. E **64**, 036304 (2001).

[52] X. L. Qiu, X. D. Shang, P. Tong, and K.-Q. Xia, "Velocity oscillations in turbulent Rayleigh–Bénard convection," Phys. Fluids **16**, 412 (2004).

[53] X. L. Qiu and K.-Q. Xia, "Viscous boundary layers at the sidewall of a convection cell," Phys. Rev. E **58**, 486 (1998).

[54] J. Wang and K.-Q. Xia, "Spatial variations of the mean and statistical quantities in the thermal boundary layers of turbulent convection," Eur. Phys. J. B **32**, 127 (2004).

[55] K.-Q. Xia, C. Sun, and S. Q. Zhou, "Particle image velocimetry measurement of the velocity field in turbulent thermal convection," Phys. Rev. E **68**, 066303 (2003).

[56] S. Ashkenazi and V. Steinberg, "High Rayleigh number turbulent convection in a gas near the gas-liquid critical point," Phys. Rev. Lett. **83**, 3641 (1999).

[57] J. M. Rensen, S. Luther, and D. Lohse, "Velocity structure functions in turbulent two-phase flows," J. Fluid Mech. (to be published).